

Article

Not peer-reviewed version

Land Use Land Cover Change Detection using Remote Sensing and Random Forest Model

Lingye Tan , Robert. L.K Tiong , [Ziyang Zhang](#) ^{*} , [Mohammad Najafzadeh](#)

Posted Date: 30 August 2023

doi: 10.20944/preprints202308.2000.v1

Keywords: spatial pattern; land use/land cover dynamic change; transition; remote sensing; driving factors



Preprints.org is a free multidiscipline platform providing preprint service that is dedicated to making early versions of research outputs permanently available and citable. Preprints posted at Preprints.org appear in Web of Science, Crossref, Google Scholar, Scilit, Europe PMC.

Copyright: This is an open access article distributed under the Creative Commons Attribution License which permits unrestricted use, distribution, and reproduction in any medium, provided the original work is properly cited.

Article

Land Use Land Cover Change Detection Using Remote Sensing and Random Forest Model

Lingye Tan ¹, Robert L.K. Tiong ¹, Ziyang Zhang ^{1,*} and Mohammad Najafzadeh ²

¹ School of Civil and Environmental Engineering, Nanyang Technological University, 639798, Singapore

² Department of Water Engineering, Faculty of Civil and Surveying Engineering, Graduate University of Advanced Technology, Kerman, Iran

* Correspondence: z.z16398741258@hotmail.com

Abstract: Land use and land cover (LULC) datasets for Jinan in 1992, 1998, 2002, 2006, 2011, 2017, and 2022 were developed from Landsat images using the Random Forest (RF) classification approach. The relationships between social-economic, political factors and time-series LULC data were examined for the periods between 1992 and 2022. The results showed the effectiveness of using the RF classification method for LULC classification with time series of Landsat images. Combined with driving forces analysis, our research can effectively explain the detailed LULC change trajectories corresponding to different stages and give new insights into Jinan LULC change patterns. The results show a significant increase in impervious surface which opposite change to bare land which experienced a huge decline declined by 95%, due to urbanization and rapid increase of population. The driving forces behind these changes are related to population growth, economic development, and climate change. Moreover, the present research employed Principal Components Analysis (PCA) methodology in order to understand the relative significance of disparate driving factors. The analysis results prove that the economy (population, GDP) and climate change were the primary factors that have an obvious impact on land use/land cover changes and that the driving factors for impervious surface, bare land, woodland, farmland, and water were distinct. Government policies also have a substantial impact on LULC change as well, such as the Construction of Harmonious Jinan (COHJ). The results were helpful for better understanding the mechanisms of LULC change and can provide useful knowledge for effective land resource management and planning.

Keywords: spatial pattern; land use/land cover dynamic change; transition; remote sensing; driving factors

1. Introduction

The alteration of land use/land cover (LULC) is the most direct indication of the impact of human activities on the Earth's surface system and plays a crucial role in the process of global environmental change [1–3]. Through interactions with the biosphere and atmosphere, human activities directly or indirectly influence surface albedo, surface energy, surface roughness, and evapotranspiration, leading to significant effects on the surface radiation energy balance, biogeochemical cycles, and ecosystem services [4,5]. Additionally, LULC is a critical factor in determining human responses to global change and serves as a vital input parameter for simulating global climate and biogeochemical effects. Understanding its spatiotemporal process and dynamic mechanism and accurately measuring and simulating its changes have become a top priority in scientific research. Apart from the influence on the natural environment, the phenomenon of LULC changes. It is of utmost significance to comprehend the changes in LULC as it plays a critical role in both short-term and long-term planning and management strategies [6–8]. The alteration of LULC patterns can result from a plethora of driving forces, including urbanization, economic growth, and natural calamities, among others. As a result, it is imperative to study the changes in LULC at both the temporal and

spatial scales to gain a comprehensive understanding of the underlying mechanisms driving these changes. The temporal analysis focuses on the examination of LULC changes over time, including the evolution of the extent and distribution of various LULC types. Contrarily, the spatial analysis examines how various LULC types are arranged and patterned, as well as how they relate to one another. In China, research on LULC has primarily focused on examining the changing patterns, driving mechanisms, and environmental impacts of land use at the regional level [9–11]. The selected areas typically fall into two main categories. The first category comprises "fragile areas" characterized by vulnerable ecological environments, often found in unique geographic locations such as coastal areas [12], plateaus [13], or delta regions [14]. The second category includes "hot spot areas" with high levels of human activity and natural drivers, often found in international metropolis like Beijing, Shanghai, and Guangzhou [15–17]. The diverse purposes and patterns of land use lead to changes in LULC, influenced by various factors. Understanding the forces driving land-use change is crucial to address land system-related challenges. Scholars have different views regarding these factors, generally classifying them into natural geographic and socio-economic factors [18–20]. Some researchers emphasize demographic factors such as population growth [21–23], population density [24,25], and rural-to-urban migration as key drivers of LULC change [26,27]. On a macro-scale, factors like climate change and soil processes play significant roles but tend to have long-term and stable effects, accumulating over time. At the regional level, socio-economic factors have a more pronounced impact [28–31].

Remote Sensing (RS) has become a reliable monitoring tool for LULC changes due to increasingly diverse and high-quality RS databases that meet various research needs. The availability of MODIS, Landsat, and Sentinel images has made RS imagery interpretation research more efficient and cost-effective. Academic studies show that image processing and classification methods have improved accuracy [32–35]. Numerous studies at local, national, continental, and global scales show that remote sensing and spatial analysis in geographic information systems enable fast and efficient land cover and LULC change detection. Some studies examined local areas [36–38], while others examined national issues [39,40]. Overall, the amalgamation of remote sensing and spatial analysis techniques in geographic information systems, coupled with advancements in image processing and classification techniques, has simplified and made the monitoring of land-use changes more cost-effective.

Jinan, the capital of Shandong Province and one of China's 14 mega cities, holds a strategic geographical position, situated between the capital economic circle in the north, the Yangtze River Delta economic circle in the south, the Shandong Peninsula in the east, and Central China in the west. Benefiting from substantial national resources and favorable policies, Jinan has experienced rapid development in recent years, becoming a prominent example of swift urbanization and industrialization over the last three decades. In 2021, with the approval of the State Council, Jinan's new and old kinetic energy conversion starting area will become the second starting area in China after Xiong'an New Area. In 2022, Jinan's GDP grew by 3.1% year-on-year, and the economic growth rate is 0.1% higher than the national average rate, which ranks eighth among all cities. The Warton Institute of Economics released the 2022 China Top 100 Cities Ranking. Jinan, serving as the capital of Shandong Province, holds the distinction of being categorized as a quasi-first-tier city, ranking 14th nationwide and standing as the foremost city within Shandong province. The city's rapid urbanization and economic growth have significantly altered the spatial and temporal patterns and attributes of land use changes in Jinan.

While research on land use change is prevalent, the current studies investigating the characteristics of land use change in China have predominantly centered on first-tier cities like Beijing, Shanghai, and Guangzhou [15–17], as well as on a national scale [41,42]. In addition, previous research on the Jinan region mainly focused on various ecosystems and specific resources, such as examining the changes in groundwater supply in the Jinan spring area. However, there is relatively little research on land use/land cover change in Jinan region [43]; atmospheric particulate pollution to LULC [44]. While less work has focused on long time series of LULC change and analysis with driving factors. In addition, the policies and regulations issued by the government are also one of the

factors that cannot be ignored in affecting sudden land use changes [45]. Numerous scholars have highlighted the significance of institutional elements, particularly local government policies [25,46,47], rules and regulations [23,48,49], and alternations in the ownership of land [50–52] can influence the trends of cities development. However, few scholars have taken policy factors into account in land research in Jinan region. Thus, it is meaningful to filling research gaps and valuable to analysis the LULC change with the past three decades and analysis several aspect factors including policies behind these changes

Random Forest (RF) model is just a classification method that we selected because it has demonstrated greater accuracy than other popular classifiers, such as Support Vector Machine (SVM), K-Nearest Neighbor (KNN) or Multi-Label Classification (MLC) in many applications [1,2], that is why we chose it as this articles classification. Additionally, the classification result showed the effectiveness with good accuracy (eg. classification accuracy exceeded 93%, Kappa Coefficient [KC] value more than 85%). In this study, the primary goal is to focus on practical applications of RF model in land use research in Jinan region and find the LULC pattern and main causes behind these changes which could provide references for some Local government and information for the urban planning and land management. On the other hand, this study is not aimed at finding new classification method, nor improve its performance by adjusting the setting parameters nor combining with other machine learning method.

The study delivers detailed information on Jinan's LULC change characteristics between 1992 and 2022. Land resource management department can create planning strategies based on the quantitative and spatial variations of LULC. These strategies aim to detect the regional properties of land use/land cover variations and optimize the utilization of farmland, forest, bare land, and impervious surfaces accordingly. In addition, farmland and woodland should be protected to encourage sustainable development in Jinan, lessen farmland fragmentation, and enhance the woodlands in terms of quality (refers to condition and characteristics of the woodland such as the health and diversity of tree species, the density of trees, the age structure of the forest) and quantity (refers to the ex-tent or size of the woodland). Additionally, finding the main LULC driving factors can spur land management organizations to develop focused land control plans. it is anticipated that the study's findings will deepen our understanding of how they changes and what impact they have, offering insightful information for efficient land resource management and planning. Hence, the primary goals of this article are: (i) to analyze and depict the primary land use and land cover (LULC) changes in the Jinan region 30 years period beginning at 1992; (ii) to investigate the impact of major driving factors, such as GDP or Population, on these LULC changes; and (iii) to assess the key implications of these changes by employing statistical methods and analyzing them in the context of national and local policies.

2. Study area and datasets

2.1. Study Area

Jinan (36° 40' N, 116° 57' E) is the provincial capital of Shandong (Figure 1). It is situated in the province of Shandong's northwestern region. The city is located in a region that divides the Yellow River valley from the northern foothills of the Taishan Massif. Numerous artesian springs can be found throughout the metropolitan area thanks to karst aquifers in limestone formations that slope north to south. A humid continental climate and a normal isotherm of 3 °C result in a yearly average temperature of 14.70 °C (58.5 °F) for Jinan. This city has direct control over six districts (Shizhong, Lixia, Tianqiao, Huaiyin, Licheng, and Changqing), one county-level city (Zhangqiu), and three counties (Pingyin, Jiyang, and Shanghe). All districts are depicted in the following figure.

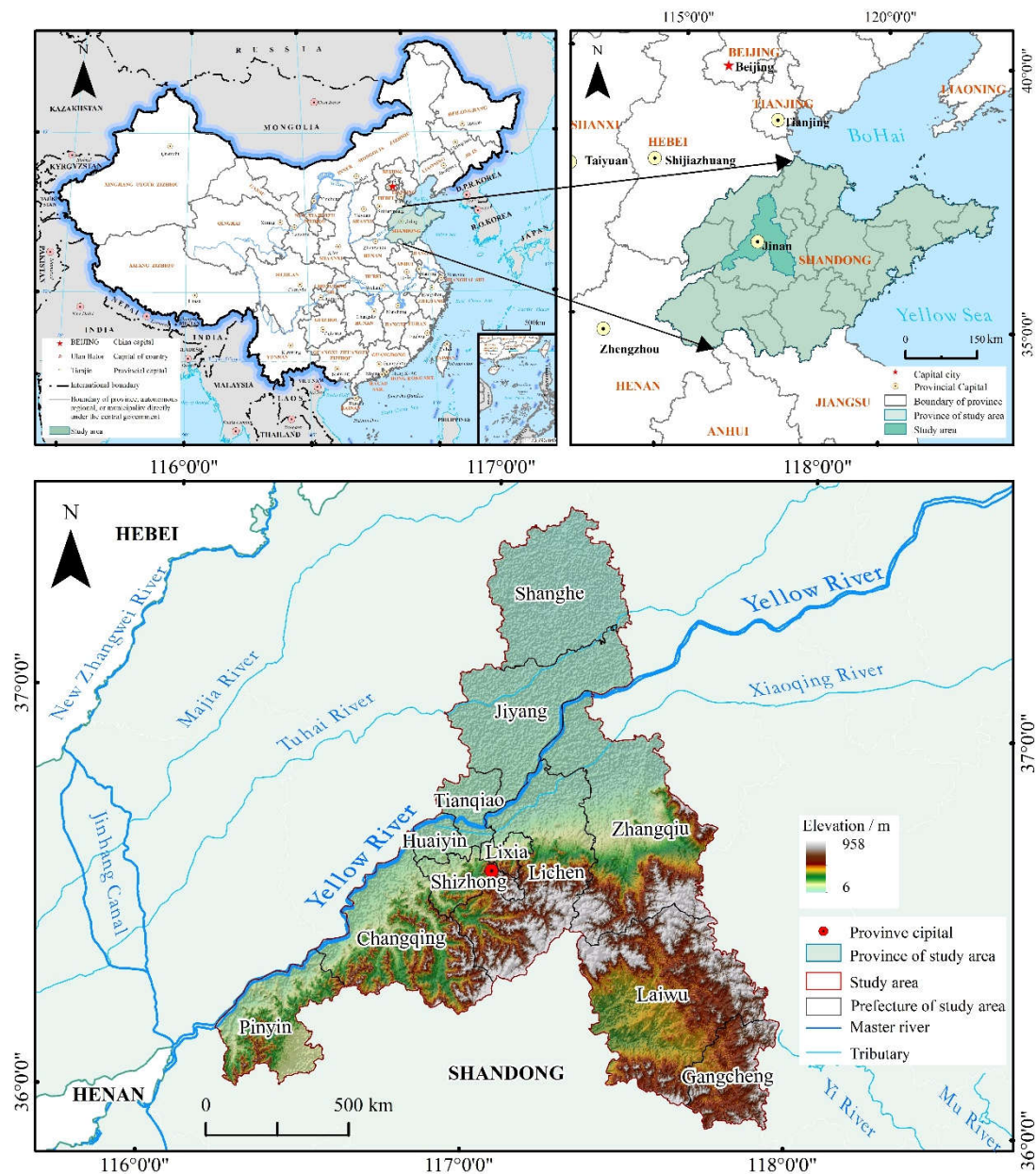


Figure 1. Research area map.

2.2. Dataset acquisition

The USGS Earth Explorer, accessible through the official website earthexplorer.gov, provides the essential satellite data (Landsat-8 OLI, Landsat-5 TM) required for analyzing changes in land use and land cover (LULC) in Jinan. The Landsat-5 TM data and the Landsat-8 OLI data offer a 30 meters resolution. In the present research, less than 5% of the satellite imagery data consists of land cloud cover and scene cloud cover. To ensure greater accuracy in determining the period, the period from April to September is generally selected as the weather is generally good and the cloud content is low. Additionally, all satellite imagery data include cloud cover below 5% which can plummet differences between months and improve the precision of classification process by Random Forest (RF). In this research, seven images were downloaded from USGS which are related to Landsat 5-TM (Type1) and Landsat 8-OLI (Type2). Information related to Band1-Band7 (B1-B7) of Type1 is used whereas for Type2, B1-B11 is applied. What is more, the coordinate system and geographical coordinate system for all images are UTM_Zone_50N and GCS_WGS_1984, respectively. Some useful information about images is presented in Table 1.

Table 1. Comprehensive details of the Landsat satellite imagery applied in this research.

Acquirement date	Source of data	Data set	resolution(m)	Cloud cover	Band	Geographical coordinate system	Projection coordinate system
27/05/1992	USGS	Landsat 5-TM	30	<5%	B1-B7	GCS_WGS_1984	UTM_Zone_50N
	USGS	Landsat 5-TM	30	<5%	B1-B7	GCS_WGS_1984	UTM_Zone_50N
28/05/1998	USGS	Landsat 5-TM	30	<5%	B1-B7	GCS_WGS_1984	UTM_Zone_50N
	USGS	Landsat 5-TM	30	<5%	B1-B7	GCS_WGS_1984	UTM_Zone_50N
23/05/2002	USGS	Landsat 5-TM	30	<5%	B1-B7	GCS_WGS_1984	UTM_Zone_50N
	USGS	Landsat 5-TM	30	<5%	B1-B7	GCS_WGS_1984	UTM_Zone_50N
02/05/2006	USGS	Landsat 5-TM	30	<5%	B1-B7	GCS_WGS_1984	UTM_Zone_50N
	USGS	Landsat 5-TM	30	<5%	B1-B7	GCS_WGS_1984	UTM_Zone_50N
16/05/2011	USGS	Landsat 5-TM	30	<5%	B1-B7	GCS_WGS_1984	UTM_Zone_50N
	USGS	Landsat 5-TM	30	<5%	B1-B7	GCS_WGS_1984	UTM_Zone_50N
16/05/2017	USGS	Landsat 8 OLI	30	<5%	B1-B11	GCS_WGS_1984	UTM_Zone_50N
	USGS	Landsat 8 OLI	30	<5%	B1-B11	GCS_WGS_1984	UTM_Zone_50N
30/05/2022	USGS	Landsat 8 OLI	30	<5%	B1-B11	GCS_WGS_1984	UTM_Zone_50N
	USGS	Landsat 8 OLI	30	<5%	B1-B11	GCS_WGS_1984	UTM_Zone_50N

Data regarding these driving factors were derived from the Jinan Municipal Bureau of Statistics(<http://jntj.jinan.gov.cn/>). Regional LULC change is caused by a variety of causes, according to research. LULC change is primarily impacted by the rise of the development cities and the economical states [53]. High correlations between the amount of developed land and arable land in a region and its economic growth have been found[54]. China has a dual urban-rural structure, and as a result, the infrastructure, employment opportunities, educational attainment, and access to healthcare in urban and rural areas differ significantly. These variations encourage rural residents to relocate to urban areas, which is a primary factor in the change in regional LULC. Therefore, we selected the three main factors that determine the population: Permanent Population (PP), Urban Population (UP), and Population Density (POD). As a result of the economy's growth and increasing salaries, the government made facility investments and raised the living standard in urban districts, which raised the area available for impervious surface and decreased the amount of farmland. Likewise, the expansion of residential construction and infrastructure would substantially boost investment in fixed assets (FAI). As a result, we settled on GDP and FAI as the key factors at the level of economic development. In addition, climate change can also affect LULC, such as the selection and scope of farmland and forest land. We select Annual Temperature (AT) and Annual Rainfall (AR) as the driving forces at the level of climate change. The annual GDP value added signifies the level of economical enhancement (unit: 109 yuan). Furthermore, other factors such as (i.e., Urban Population [UP], Population Pressure [PP], Population Density [POD], Urban Income [UI], Farmers Income [FI]) are listed in Table 2.

Table 2. Statistical summary of the independent factors related to land-use variation.

Factors	Description
Population Pressure (PP)	The total registered population of the city each year; represents population pressure (unit: 10 ⁴)
Urban Population (UP)	Population residing in the urban area each year; represents urbanization level (unit: 10 ⁴)
Population Density (POD)	Residences per area; a measure of population pressure (unit: /km ²)

Urban Income (UI)	Represents the capacity to improve urban residents' living conditions (unit: yuan)
Farmers Income (FI)	Represents the capacity to improve farmers' living conditions (unit: yuan)

2.3. Pre-processing stage of Images

Due to the errors of the sensor itself and the refraction or absorption of the solar radiation entering the atmosphere, all of the factors will produce different degrees of impact on the received signal of the sensor, so a series of pre-processing should be performed before applying the remote sensing images of the study area, to improve the accuracy of the interpretation. In this study, we use ENVI 5.3 to do image processing, which contains several steps: Radiation calibration, Atmospheric correction, Image mosaic, and Image cropping. In Figure 2, the entire LULC workflow is depicted.

Radiometric calibration, also referred to as radiometric correction, is essential for successfully converting unprocessed digital image data from satellite or aerial sensors to a typical physical scale based on known reflectance measurements acquired from objects' surfaces on the ground[55]. This type of correction is essential for obtaining accurate quantitative assessments of imagery. The objective of atmospheric correction is to eliminate atmospheric effects from remote sensing satellite images, allowing for the retrieval of surface reflectance. This crucial process is essential for quantitative remote sensing, as it reduces atmospheric interference. Problems with atmospheric disturbance are resolved by using the FLAASH (Fast Line-of-Sight Atmospheric Analysis of Spectral Hypercubes) atmospheric correction technique, which eliminates absorption brought on by the effects of CO₂, O₂, O₃, and water vapor as well as scattering brought on by molecules and aerosols[56]. When extracting information from imagery data obtained under different conditions based primarily on spectral features, such as when detecting changes or mapping vegetation using extensive multitemporal Landsat imagery data, atmospheric correction is particularly crucial. Image mosaic and Image cropping are the processes of stitching multiple adjacent images that contain part of the study area into one image that completely covers the study area, and then cropping the desired area according to the study boundary data.

Additionally, a single remote sensing map cannot completely cover the whole study area, we stitch the two remote sensing maps after radiometric calibration and FLAASH into one map that can completely cover the study area. And this function is achieved by the function of SeamlessMosaic in ENVI5.3. To create the final area map that can be used for the classification that follows, the stitched image is cropped in accordance with the vector boundary of the study area.

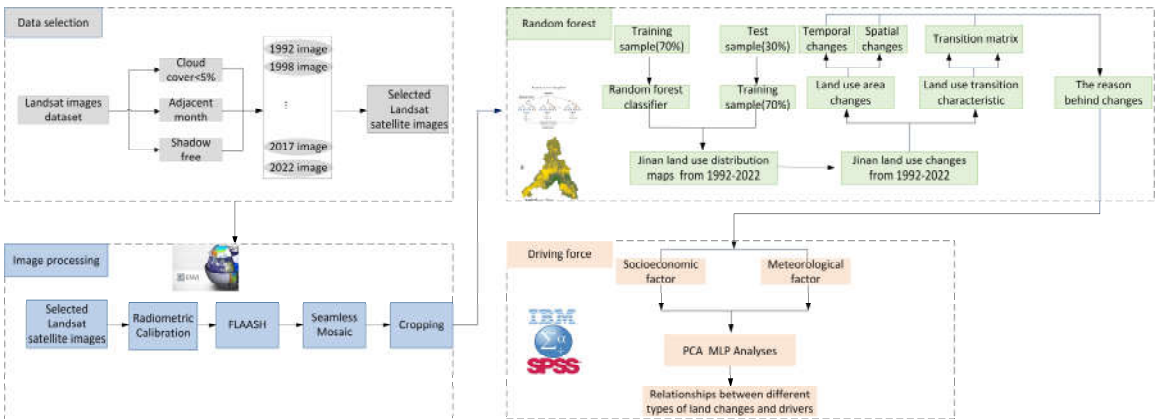


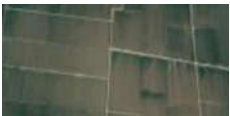




Figure 2. Workflow of LULC change based on Random Forest classification.

3. Methods

3.1. Image Interpretation

The Jinan City region consists of farmland (wheat, rice, sugarcane, etc.), forest, urban and rural impervious surface, and water bodies (rivers, canals, and ponds). Five LULC classes have been determined for this study after a review of the literature. Using the ENVI 5.3 Tool, the Set of training area classes is created by selecting polygons for each class. The spectral properties and response are used to separate these LULC classes. The ROI (region of interest) tool is utilized for assessing spectral variations within defined pairs of LULC classes and demonstrates significant levels of separability between regions of interest. Table 3 displays remote sensing image interpretation symbols.

Table 3. Remote Sensing Image Interpretation Symbols.

No.	Classification types	Implications	Image example	Image features
1	Farmland	Land on which crops are grown, including watered land, dry land, grassland, shrubs		True color images are green and divided into blocks of regular shapes by roads, generally surrounded by residential areas
2	Impervious surface	Includes urban sites and villages		Standard false-color images show red with white dots and grey with blue, both in aggregates
3	Water	Including rivers, lakes, and ponds		Dark blue on standard false color images, curved or irregularly shaped
4	Woodland	Woodland and other forestlands		Red and irregularly shaped on standard false color images, distributed in mountainous areas
5	Bare land	Low-coverage areas, unused land		Irregular brownish-yellow color on true color images, mostly located in mountainous areas

3.2. Random Forest Classification

When classifying land cover using remote sensing data, RF is currently regarded as one of the most popular techniques [57–60]. The explanations for RF receiving significant enthusiasm over the last two decades are—(1) Good performing of the outliers and noisier datasets; (2) Good performance with high dimensional and multi-source datasets; (3) Greater accuracy than other popular classifiers, such as SVM, KNN or MLC in many applications[61,62]; and (4) Promoting the processing speed by selecting important variables [63]. Compared with other most well-known ML models, key advantages of RF model are presented as follows:

reduced overfitting, improved accuracy by combining the predictions of multiple trees in comparison with single decision trees, handling non-linearity when facing dealing with complex datasets, robustness to Outliers by averaging of predictions from multiple trees for reduction of the impact of outliers, feature importance, handling missing values, reduction of bias values by averaging the predictions of many trees with different initializations and training subsets, less hyperparameter tuning, and reduction of variance.

Random Forest is a machine learning algorithm that falls under the category of supervised learning. In supervised learning, the algorithm learns from a labeled dataset, where the input data is associated with corresponding target labels or outcomes. The goal is to learn a mapping from inputs to outputs, so the algorithm can make predictions on new, unseen data. Random Forest is made up of several classifiers in which each classifier contributes one vote to the most frequent class assignment for the input vector (x),

$$\hat{C}_{rf}^B = \text{majorityvote}\{\hat{c}_b(x)\}^B \quad (1)$$

where:

$\hat{c}_b(x)$ is the prediction value of the b_{th} tree.

RF differs significantly from the conventional classification tree (CT) due to the specificity provided by the fact that it is a mixture of numerous classifiers. As a result, it should be viewed as a distinct classifier idea. RF creates more diverse trees by combining various training data subsets via bagging or bootstrapping [64], which also modifies the sample distribution of the data used by the model, introduces noise, and improves the model's generalization ability. During this process, a random sample of the original data set is used in place of the original data in this procedure (i.e., does not remove selected data from the input sample to create the next subset). Random forest (RF) is an ensemble classification technique that employs a tree as its fundamental classifier.

$$\{h(x, \Theta_k), k = 1, \dots, \} \quad (2)$$

With x being the input vector and $\{\Theta_k\}$ being a random vector that is independently and uniformly distributed [64,65]. In addition, each tree grows without being pruned. After the tree has completed its growth, only a few variables are generated at random for each node's variables. As a result, certain data may be utilized more than once in training the classifier, while other data may never be utilized. In other words, both the samples and variables used are randomized, and this double randomization process is resistant to overfitting. By being more resistant to subtle changes in the input data, the classifier becomes more stable. Additionally, the classification's accuracy is increased [64].

In this article, we conducted Random Forest by ENVI software and all parameters are set as following: n_ Estimators=400; Impurity Function: Gini Index; Minimum impurity threshold=0; Minimum number of samples=1.

3.3. Classification Accuracy Validation

The confusion matrix is a widely accepted evaluation tool in the field of LULC classification that provides a visual representation of the agreement between predicted and actual classifications. By using the confusion matrix, it is possible to offer a quantitative measure of accuracy, providing the ability to compare results with other classifications or previous results[66].

To ensure correctness, the ground truth data was matched to the categorized image. To assess categorization accuracy, the user and producer accuracy was tested. The accuracy of the producer is determined by dividing the total number of correctly categorized pixels. The inaccuracy of misclassified pixels, as well as misclassification into a different class, was recorded. In the meantime, the user's accuracy is a measurement of the individual class acquired from the pixels classified in the same group[67]. The confusion matrix produced for user and producer accuracy was used to calculate the total accuracy. User accuracy (UA), producer accuracy (PA), and overall accuracy (OA) are described below.

User accuracy and producer accuracy are two important performance metrics that are derived from the confusion matrix in the evaluation of LULC classification accuracy. User accuracy is the percentage of samples correctly categorized by the classifier relative to the actual sample class. It is calculated as the amount of correctly classified samples (i.e. True Positives) divided by the total number of samples (i.e. True Positives plus False Negatives). Producer accuracy, on the other hand, is defined as the proportion of samples in a particular class that was correctly classified by the classifier. It is calculated as the number of samples that were correctly categorized (i.e. True Positives) divided by the total number of samples that were classified as that particular class (i.e. True Positives plus False Positives).

Both user accuracy and producer accuracy are commonly used to evaluate the performance of LULC classification algorithms. However, it is important to note that while user accuracy measures the overall accuracy of the classification, producer accuracy provides a class-specific evaluation of accuracy.

$$User\ Accuracy(UA) = \frac{(Number\ of\ True\ Positive + Number\ of\ True\ Negative)}{(Number\ of\ True\ Positives + Number\ of\ False\ Negatives)} \times 100 \tag{3}$$

$$Producer\ Accuracy(PA) = \frac{Number\ of\ Ture\ Positive}{(Number\ of\ True\ Positives + Number\ of\ False\ Positive)} \times 100 \tag{4}$$

where True Positives represent the count of pixels that are correctly classified as positive. True Negatives denote the quantity of pixels that are accurately classified as negative. False Negatives refer to the pixels that are incorrectly classified as negative, but they should have been classified as positive. Additionally, False Positives represent the pixels that are incorrectly classified as positive, but they should have been classified as negative. Total Pixels is the total number of pixels in the image

$$Overall\ Accuracy(OA) = \frac{Total\ number\ of\ correct\ classified}{Total\ number\ of\ pixels} \times 100 \tag{5}$$

The Kappa Coefficient (KC) is an additional metric used to compare training pixels with ground truth data. It measures the extent of agreement beyond chance by comparing the observed agreement between classification results and reference data to the expected agreement. Kappa values range from +1.0 to -1.0, with values above 0.7 indicating substantial agreement [65]. A value of zero suggests no correlation in categorization. Typically, the KC is used alongside other metrics like overall accuracy, user accuracy, and producer's accuracy to offer a comprehensive evaluation.

$$Kappa\ Coefficient = \frac{n \sum_{i=1}^p x_{ii} - \sum_{i=1}^p x_{i0} x_{0i}}{n^2 - \sum_{i=1}^p x_{i0} x_{0i}} \tag{6}$$

where:

- n = total number of pixels
- p =number of classes
- $\sum x_{ii}$ =total number of elements of the confusion matrix
- $\sum x_{i0}$ =sum of row i
- $\sum x_{0i}$ =sum of column i

Table 4. LULC/land cover classification accuracy from 1992 to 2022.

Classification Category	User Accuracy	Producers' Accuracy
Impervious surface	[84.85%,96.43%]	[97.91%,100%]
Water	[99.15%,100%]	[84.31%,98.59%]
Farmland	[66.41%,99.42%]	[86.99%,100%]
Woodland	[80.57%,99.17%]	[91.26%,99.97%]
Bare land	[74.48%,100%]	[20%,100%]
Overall Accuracy	[93.7561%, 98.1314%]	Kappa Coefficient [0.8686, 0.9741]

3.4. Method of LULC change

For the analysis of various types of land-use change and to determine its rate, we employed four indicators. These indicators include the net total change area, annual change area, annual change rate, and dynamic degree.

In order to compute the annual change rate (K_i) related to land-use type i , the following equation is expressed,

$$K_i = \frac{\Delta s_{i,j}}{s_i} \times \frac{1}{t} \times 100\% \tag{7}$$

In the given context, s_i represents the initial area of land-use type i at the beginning of monitoring. $\Delta s_{(i,j)}$ denotes the total net area of changes between land-use types, where j changes to or

from land-use type i during the time period t . K_i is calculated for the case study over the time period t .

Eq.(8) is utilized to calculate the dynamic degree (L) of i :

$$L = \frac{\sum_{i=1}^n |s_i - s_j|}{\sum_{i=1}^n s_i} \times \frac{1}{t} \times 100\% \quad (8)$$

in which, s_i represents the area of a specific land type at the start of the study, while s_j represents the area of the same land type at the end of the study. The variable n corresponds to the total number of land types ($n=1,2,3,\dots$), and t represents the time duration of the study case.

3.5. Land-Use Transfer Matrix

In this research, the area of six distinct LULC types was utilized to compute the land-use transfer matrices for seven time periods from 1992 to 2022 in Jinan City. The land-use transfer matrix (LUTM) [66] is an extension of the Markov transfer matrix, initially used to describe transitions from one state to another over a specific period. It has been widely employed in academic literature to gain deeper insights into the evolution of land-use change [67] and is particularly useful in describing the conversions between various land-use types [68]. The calculation was performed using ArcGIS 10.2.2, and the LUTM calculation equation is provided below.

$$S_{ij} = \begin{bmatrix} s_{11} & s_{12} & \dots & s_{1n} \\ s_{21} & s_{22} & \dots & s_{2n} \\ \dots & \dots & \dots & \dots \\ s_{n1} & s_{n2} & \dots & s_{nn} \end{bmatrix} \quad (9)$$

where S_{ij} is the area represents the area transformed from land-use type i to land-use type j ; At the start and the end of the study period, i and j denote the specific land-use type, and n denotes the total number of land-use types. The land use transfer matrix (Introduced as Eq.(9)) is a two-dimensional matrix obtained based on the changes in land cover status at different times in the same region. By analyzing the obtained transfer matrix, we can obtain the mutual transformation between two different land types in different time periods. It describes the land types that have undergone changes in different years, as well as the location and area of the changes. Not only can it reflect the static fixed area fixed time area data of various land types mentioned above, but it can also reflect a more abundant initial area transfer of each land type and the final area transfer of each land type. In most cases, a certain type of land is not simply converted to another land type, but rather to multiple land types.

3.6. Driving Forces of LULC change

The interaction of human activity and the natural environment leads to land-use change, which is a crucial aspect of regional sustainable development[68,69]. Human activities have surpassed the constraints imposed by the physical geography of the planet by implementing advanced farming methods and engineering solutions like land consolidation, which have changed the geographic distribution and type of regional LULC[70]. Land-use change is primarily driven by human activities related to urbanization, population rise, and land-use/land-cover (LULC) management policies. These factors have indirect effects on LULC [72]. The Principal Components Analysis (PCA) was employed to calculate the principal component using the following variables: total annual precipitation, mean temperature, gross domestic product, total population, urban population, resident population per unit area, urban people's income, farmer income, and fixed asset investment. (Supplementary Table S2). During the period 2000–2020, we collected each data set on an annual basis for the purposes of pre-processing. SPSS was utilized to conduct the principal component analysis.

This study introduces a "two-step" analytical approach. Initially, all identified factors from the general LULC analysis undergo a principal component analysis. In the second step, the key variables

are identified within the significant dimensions, and stepwise regression modeling is conducted to assess the interaction between typical LULC and these essential variables.

3.6.1. Principal Components Analysis

To examine the factors influencing land-use and land-cover (LULC) change, we included a range of socioeconomic and natural climate indicators. However, there might be significant correlations (informational overlap) among these various indicators. To address this issue, we initially filtered the variables using principal components analysis.

Principal components analysis (PCA) is a multivariate statistical technique used to assess the level of correlation among different variables. It replaces the initial variables with a new set of composite variables that are uncorrelated by combining multiple variables with specific correlations. The primary goal is to retain as much information as possible while reducing the dimensionality of the variable dataset. This is achieved by orthogonally transforming a set of potentially correlated variables into a new set of linearly independent variables, with the top few variables retaining the majority of the variance present in the original variables [73]. These transformed variables are referred to as principal components and are used in subsequent analyses.

In mathematical terms, let's assume that there are n samples of x , and each sample consists of p variables. We can represent this as a matrix of dimensions $n \times p$.

$$X = \begin{bmatrix} x_{11} & x_{12} & \dots & x_{1p} \\ x_{21} & x_{22} & \dots & x_{2p} \\ \dots & \dots & \dots & \dots \\ x_{n1} & x_{n2} & \dots & x_{np} \end{bmatrix} \quad (10)$$

These comprehensive indices were obtained by applying a linear transformation to this variable respectively: z_1, z_2, \dots, z_m ($m \leq p$)

$$\begin{cases} z_1 = l_{11}x_1 + l_{12}x_2 + \dots + l_{1p}x_p \\ z_2 = l_{21}x_1 + l_{22}x_2 + \dots + l_{2p}x_p \\ \dots \\ z_m = l_{m1}x_1 + l_{m2}x_2 + \dots + l_{mp}x_p \end{cases} \quad (11)$$

In recent equation, the coefficient l_{ij} is defined with aid of two main principles: (i) z_i is not influenced by z_j , and (ii) z_1 exhibits the highest variance among all linear combinations, while z_m displays the lowest variance. The new variables (i.e., z_1, z_2 , and z_3) represent the first, second, and third principal components of the original variables. In practical applications, to simplify the relationship between variables, the top few principal components with the highest variances are often utilized.

3.7. Multiple Linear Regression Analysis

The multiple stepwise technique is a regression model fitting method that involves an automated procedure to repeatedly perform regression analysis and significance testing on explanatory variables. Only those variables that significantly contribute to improving the model are ultimately retained. This is accomplished by evaluating a group of explanatory factors for addition or deletion in accordance with some predetermined criteria. The following is the multiple regression model:

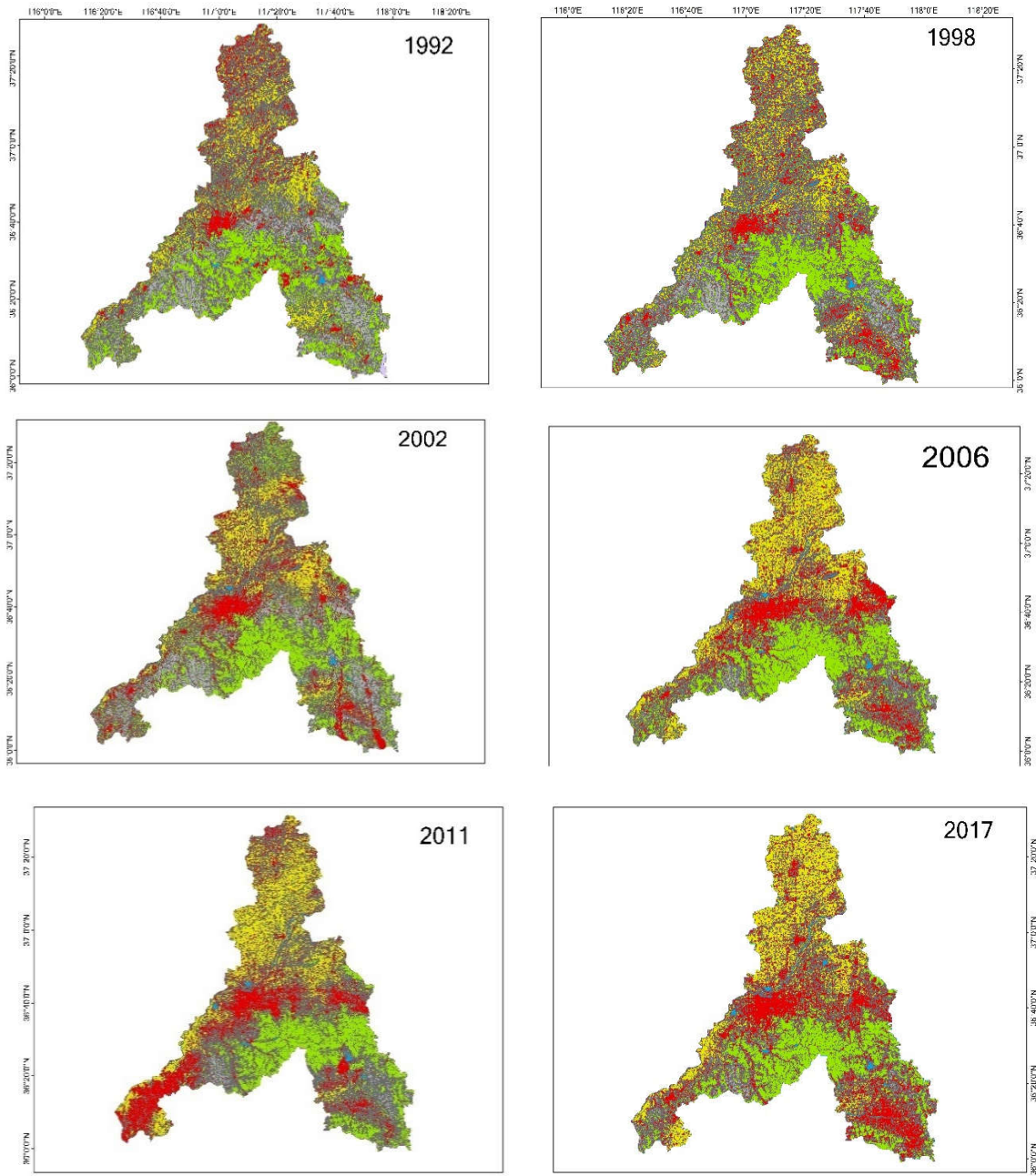
$$Y = \beta + \alpha_1 X_1 + \alpha_2 X_2 + \dots + \alpha_n X_n \quad (12)$$

where $\alpha_1, \alpha_2, \dots, \alpha_n$ denotes the weighting coefficients, and β is introduced as bias/constant term. This research performed SPSS software to implement PCA and the multiple linear regression analysis.

4. Results and analysis

4.1. Quantity and Spatial Distribution of LULC

The findings revealed significant changes in the spatial distribution of LULC in Jinan City (Figure 3). Among them, there has been a noticeable increase in impervious surface, and the southern part of the woodland has maintained its stability. Bare land declined a lot and most of the farmland is located in the northern part of Jinan City.



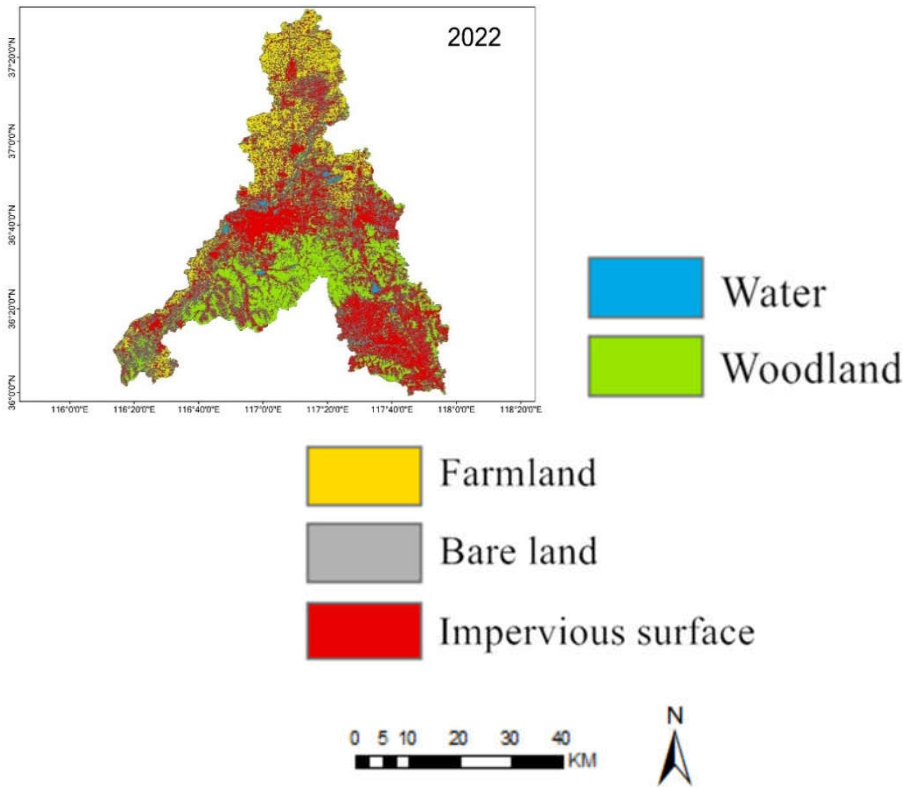


Figure 3. Land-use maps of Jinan province in the reference years.

Figure 3 and Table 5 depicts the land-use maps and areas for each type in Jinan City over seven time periods, and Table 6 lists the specific dynamics for each class from 1992 to 2022.

Table 5. Area for each type of LULC/land cover.

Area for each type of LULC/land cover(km²)							
Classification Category	Research year						
	1992	1998	2002	2006	2011	2017	2022
Impervious surface	2348.85	2663.99	2959.29	3465.73	3671.33	4059.49	4795.35
Water	81.36	90.89	77.00	121.05	89.32	117.87	127.40
Farmland	2109.92	2401.25	1933.30	2883.48	2812.43	2562.78	2103.97
Woodland	3774.52	3861.84	3587.98	3314.91	3083.91	3043.83	3088.28
Bare land	1888.05	1184.74	1645.15	421.11	550.10	422.30	91.29
Total	10202.71	10202.71	10202.71	10206.28	10207.09	10206.27	10206.28

Table 6. LULC factors of change in the reference years.

Research year	Factors of change	Impervious surface	Water	Farmland	Woodland	Bare land
1992-1998	Amount km²	315.14	9.53	291.33	87.32	-703.31
	Rate km/year	52.52	1.59	48.55	14.55	-117.22
	Ki	13.42%	11.71%	13.81%	2.31%	-37.25%
	L			2.30%		
1998-2002	Amount/km²	295.29	-13.89	-467.95	-273.86	460.41
	Rate km/year	73.82	-3.47	-116.99	-68.47	115.10
	Ki	11.08%	-3.82%	-19.49%	-7.09%	38.86%
	L			3.70%		

2002-2006	Amount/km ²	506.45	44.06	950.18	-273.07	-1227.61
	Rate km/year	126.61	11.01	237.54	-68.27	-306.90
	K_i	17.11%	57.22%	49.15%	-7.61%	-74.62%
	L	7.35%				
2006-2011	Amount/km ²	205.59	-31.73	-71.05	-231.00	128.18
	Rate km/year	41.12	-6.35	-14.21	-46.20	25.64
	K_i	5.93%	-26.21%	-2.46%	-6.97%	30.70%
	L	1.90%				
2011-2017	Amount/km ²	388.17	28.55	-249.65	-40.09	-126.98
	Rate km/year	64.69	4.76	-41.61	-6.68	-21.16
	K_i	10.57%	31.96%	-8.88%	-1.30%	-23.27%
	L	0.32%				
2017-2022	Amount/km ²	735.85	9.53	-458.82	44.45	-331.02
	Rate km/year	147.17	1.91	-91.76	8.89	-66.20
	K_i	18.13%	1.62%	-17.90%	1.46%	-79.05%
	L	3.10%				

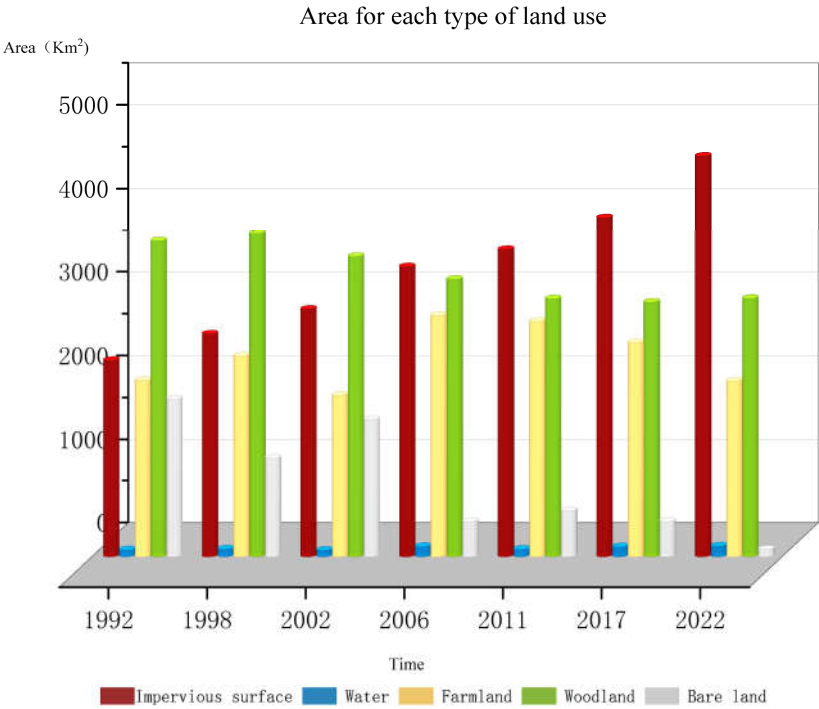


Figure 4. The areas of different types of LULC from 1992-2022.

Over the last three decades, there have been substantial changes in the land-use and land-cover (LULC) of Jinan City. Notably, there has been a significant increase in impervious surface area, while the area of bare land has decreased. The areas of farmland and bare land have experienced fluctuations, initially increasing and then decreasing, resulting in an overall decrease in their respective areas. The overall area of the water remained stable and almost unchanged; the Woodland shows a slight downward trend. In addition, the average rate of change over these 30 years was ordered as impervious surface>bare land>water>woodland>farmland. Comprehensive analysis shows that in the past 30 years, the area of impervious surface, farmland, and bare land has changed significantly, which is the main manifestation feature of LULC change in the study area.

The area of impervious surface showed a sharp and upward trend between 1992 and 2022. In 1992, the area of impervious surface only accounted for 2348km², it rose to 4795km² in 2022. This increase is likely due to the rapid urbanization and economic development in the region, which has led to an increase in the demand for land for commercial and residential purposes. To trade-off for

this expansion, the areas of bare land and woodland reduce by 1800km² and 686km² respectively. In 1992, Only in the central part of Jinan City is there a concentrated area (Lixia District and Shizhong District, about 36°40' N, 117°E), which has continuously expanded over the past 30 years. In 2022, this area almost spans the entire central administrative region (Huaiying District, Shizhong District, Lixia District, Licheng District, Zhangqiu District). The construction area of Laiwu District and Gangcheng District, located in the southeast direction, has continuously expanded, forming the second largest impervious surface area except for the central area.

During the study period, 45.63km² of water area was converted to other uses, primarily forest, construction, and agricultural land. In the meantime, 91.67km² of water surface was created, primarily from impervious surface. Consequently, despite fluctuations over time, the water surface area grew from 81.36km² in 1992 to 127.40 km² in 2022, which has always been relatively small at approximately 100 km².

On the contrary, despite receiving contributions from other land-use types, the area of bare land has consistently decreased over the past 30 years. The bare land declined by 95% between 1992 and 2022, from 1888km² to 87 km². From occupying 19% of the province's land area, it now occupies only 1%. Which, the four-year period between 2006 and 2011 experienced the most significant decline. Meanwhile, the change in bare land exists a small fluctuation in the 1992-2002 period from 1888.05 km² to 1184.74km² then 1645.15km², after 2002, there experienced a sharp decline for the first period and then became gradual decrease for the rest 16 years.

There was a fluctuation trend in woodland over the last 30 years. Its area grew from 1992 to 1998 and again from 2017 to 2022, but it shrank from 1998 to 2017. In the total 30 years, the total woodland area convert to other types of land was 686km², mainly for impervious surface. Therefore, from accounting for the biggest part about 37% of the total area in 1992, Jinan province had approximately 30% area in 2022. This decline is most likely caused by the growth of urban areas, the creation of infrastructure, and the commercial exploitation of forests. Over the past 30 years, the primary spatial distribution of woodland in Jinan City has remained largely unchanged. The majority of woodland is concentrated in the southern parts of the Changqing, Licheng, Zhangqiu, and Laiwu Districts. Further investigation revealed that the southern region is predominantly mountainous, with forested areas covering a significant portion of the landscape.

Not like the above types of land, farmland experienced growth and decline and fluctuated for 30 years. But the area in the research beginning and end was almost the same which changed from 2109.92km² to 2103.97km², and there were transformations with other types of land but the amount of transfer in and out was the same. The majority of cultivated land in Jinan City is concentrated in the northern region, where it is interspersed with clusters of impervious surfaces. While the patch-like areas of cultivated land have gradually expanded over time, the distribution remains primarily focused in the northern area.

4.2. LULC transition characteristics

The LULC transfer matrix of Jinan City was obtained by comparing the results of LULC classification in seven different periods using ENVI software, as shown in Table 6 and Figure 5. Over the past 30 years, all types of land have transformed.

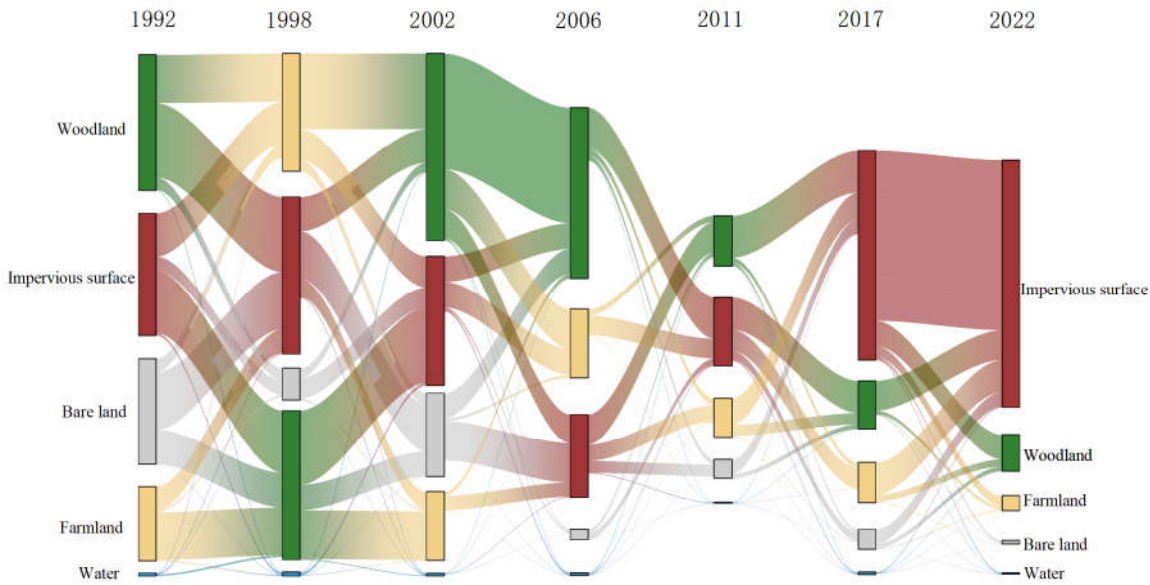


Figure 5. Sankey diagram of LULC transfer matrix.

Table 7. LULC transition matrix during 1992-2022.

<div>19981992</div>	Bare land	Impervious surface	Farmland	Water	Woodland	Total
Bare land	8.38%	1.36%	0.18%	0.00%	1.17%	11.10%
Impervious surface	5.48%	11.45%	2.27%	0.08%	7.13%	26.40%
Farmland	1.27%	4.10%	13.19%	0.03%	4.57%	23.11%
Water	0.00%	0.23%	0.10%	0.52%	0.06%	0.88%
Woodland	3.32%	5.97%	4.54%	0.17%	24.44%	38.39%
Total	18.46%	23.10%	20.27%	0.79%	37.38%	100.00%

<div>20021998</div>	Bare land	Impervious surface	Farmland	Water	Woodland	Total
Bare land	8.12%	4.53%	1.04%	0.00%	2.42%	16.11%
Impervious surface	1.96%	16.79%	2.98%	0.24%	7.15%	29.11%
Farmland	0.16%	1.72%	11.88%	0.05%	4.63%	18.42%
Water	0.00%	0.13%	0.05%	0.54%	0.08%	0.80%
Woodland	0.90%	3.25%	7.17%	0.05%	24.19%	35.55%
Total	11.14%	26.41%	23.11%	0.88%	38.46%	100.00%

<div>20062002</div>	Bare land	Impervious surface	Farmland	Water	Woodland	Total
Bare/low-cover land	3.26%	0.40%	0.06%	0.00%	0.34%	4.07%
Impervious surface	7.56%	18.51%	2.72%	0.12%	5.50%	34.42%
Farmland	0.51%	4.95%	14.78%	0.03%	7.57%	27.84%
Water	0.03%	0.37%	0.05%	0.63%	0.08%	1.15%
Woodland	4.76%	4.88%	0.81%	0.02%	22.06%	32.52%
Total	16.11%	29.11%	18.42%	0.80%	35.55%	100.00%

<div>20112006</div>	Bare land	Impervious surface	Farmland	Water	Woodland	Total
Bare land	2.07%	2.26%	0.05%	0.01%	0.94%	5.33%

Impervious surface	1.22%	23.07%	3.74%	0.20%	7.89%	36.12%
Farmland	0.11%	3.17%	22.84%	0.02%	1.30%	27.45%
Water	0.00%	0.14%	0.01%	0.69%	0.04%	0.88%
Woodland	0.66%	5.78%	1.20%	0.22%	22.34%	30.22%
Total	4.07%	34.42%	27.84%	1.15%	32.52%	100.00%
2017 2011	Bare land	Impervious surface	Farmland	Water	Woodland	Total
Bare land	1.67%	1.64%	0.17%	0.00%	0.52%	4.01%
Impervious surface	2.71%	24.03%	5.03%	0.13%	7.96%	39.87%
Farmland	0.06%	4.07%	20.06%	0.01%	0.94%	25.14%
Water	0.02%	0.26%	0.05%	0.72%	0.12%	1.15%
Woodland	0.87%	6.13%	2.14%	0.02%	20.67%	29.84%
Total	5.33%	36.12%	27.45%	0.88%	30.22%	100.00%
2022 2017	Bare land	Impervious surface	Farmland	Water	Woodland	Total
Bare land	0.29%	0.44%	0.13%	0.00%	0.12%	0.97%
Impervious surface	2.68%	32.41%	6.12%	0.21%	5.64%	47.06%
Farmland	0.17%	1.99%	17.50%	0.01%	0.66%	20.33%
Water	0.00%	0.24%	0.03%	0.92%	0.06%	1.24%
Woodland	0.87%	4.79%	1.36%	0.02%	23.36%	30.39%
Total	4.01%	39.87%	25.14%	1.15%	29.84%	100.00%

Between 1992 and 1998, approximately 14% of the Woodland had been converted to other land types, such as Bare land, Impervious surface, and Farmland. Bare land was primarily transformed into impervious surface and Woodland, while Farmland was mainly converted to impervious surface and Farmland. During this period, the area of concessions for Bare land was lower than the area of transfers, amounting to approximately 700km², while the area of concessions for other types of land was higher than the area of transfers. In particular, both Farmland and Impervious surface areas increased by approximately 13%.

Between 2002 and 2006, the largest gap between inward and outward transfers occurred for Bare land, resulting in a decrease of approximately 12% in its area. Farmland, Impervious surface, and Water were converted into each other, and the transfer volume for these three land types was higher than the transfer out. In contrast, the transfer volume for Woodland was lower than the transfer out, with most of it being converted to impervious surface. As a result, the area of Bare land and Woodland decreased during this study period, with a portion of the reduction being transformed into the other three land types.

During the three time periods of 2006-2011, 2011-2017, and 2017-2022, the area of land transfer for all types was less, except for the increase of Impervious surface in the last period. The transfer area for impervious surface exceeded the transfer out area, resulting in an 18% increase in its area between 2017 and 2022. During these three time periods, the total area of impervious surface increased while the areas of Farmland and Bare land decreased. These three types of land were converted into each other, with the Sankey diagram indicating that the transfer area for various types of land during the 2006-2017 period was lower than that of the other research periods.

4.3. Driving Force of LULC

4.3.1. Economic and Population Development

We used 9 factors such as GDP and population as input data for 30 consecutive years from 1992 to 2022, in other words, 9 * 30 sets of data are used as raw data for PCA input. Afterwards, all data

were standardized in SPSS, followed by The Kaiser–Meyer–Olkin (KMO) and Bartlett's tests. The results of this experiment were $KMO=0.775>0.5$, $P<0.05$. Therefore, these 30 sets of data have structural validity and can be used for principal component analysis.

Using principal component analysis, each of the nine indicators' change data could be reduced to two components (Table 7). The first principal component (F1) is a description of economic growth, reflecting primarily changes in the Gross domestic product(X4), Urban income (X5), Farmer income (X7), Permanent population (X1), Urban population (X2), and POD (X3). The second principal component (F2) primarily reflects annual temperature (X8) and annual precipitation (X9) to characterize regional climate change.

Table 7. Component matrix of the PCA in this research.

Factors	Variables	Component	
		F1	F2
GDP	X1	0.963	0.119
Permanent Population (PP)	X2	0.905	0.071
Urban Population (UP)	X3	0.979	0.074
Population Density (POD)	X4	0.986	-0.048
Urban income (UI)	X5	0.987	-0.048
Farmers income (FI)	X6	0.981	-0.073
Fixed assets investment (FAI)	X7	0.979	-0.067
Annual Temperature (AT)	X8	0.039	-0.766
Annual Rainfall (AR)	X9	0.015	0.795

Multiple linear regression analysis (Table 7) could be used to derive the statistical model of the relationship between changes in land area and the primary driving factors. The significance test is passed by the driving relationship models of every kind of land. The particular models demonstrated the following:

This reflects the previous expansion of construction areas, which occurred concurrently with the swift growth of the national economy and the consistent acceleration of Jinan's population growth.

Water area exhibited a negative (reverse) correlation with economic factors (F1) and a positive correlation with climate factors (F2), with F1 having the most significant influence. This implies that Jinan's economic development may lead to the encroachment of some traditional water bodies by urban and rural construction sites, although this impact is not expected to be substantial. On the other hand, climate change-related factors, such as increased precipitation, will likely result in denser water bodies in Jinan. Farmland areas had a negative correlation with the economy (F1) and a positive correlation with climate (F2). It was influenced primarily by economic expansion. As a result of this primary factor, the area of farmland will decrease to compensate for the encroachment of impervious surface expansion on traditional farmland. The woodland area had a positive correlation with climate change and a negative correlation with the economy (F1). This is a result of traditional woodland being encroached upon by urban development and impervious surface expansion, but this encroachment is not a significant factor. However, the expansion of woodlands will be brought on by climate change, particularly the increase in precipitation. The area of bare land exhibited a negative correlation with both the economy (F1) and climate change (F2), with F1 being the primary influencing factor. This suggests that the development of construction or urban expansion utilized the bare land area, resulting in significant development for construction purposes.

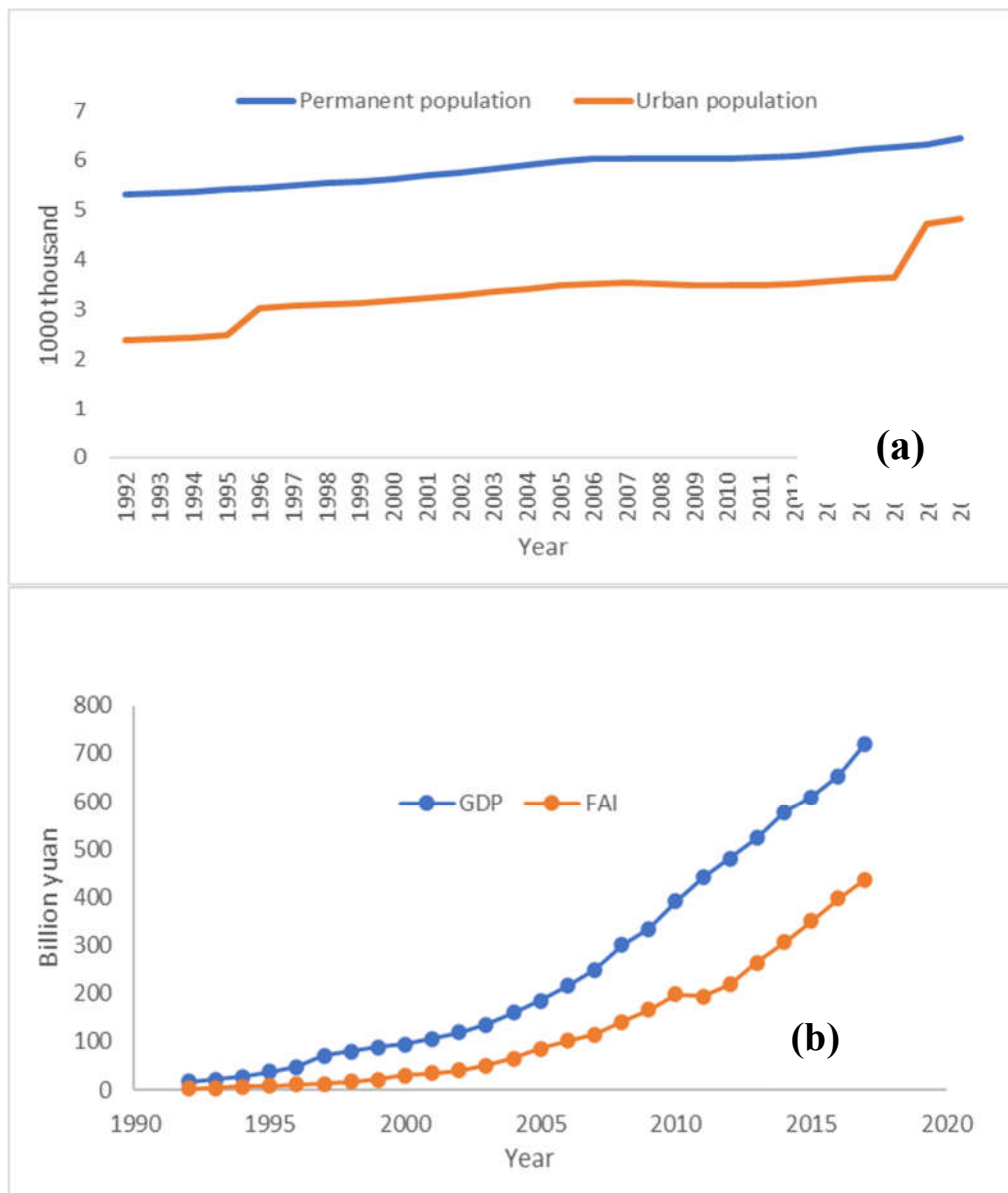


Figure 6. Variations of (a) economic factors and (b) populations in Jinan City during 1992-2017. Note: GDP, Gross Domestic Product; FAI, Fixed Assets Investment.

We referred to reference [73,61,62], which compared the accuracy of RF, Classification Tree (CT), SVM, and ANN classification methods. In [61], the accuracy level of three machine learning models (i.e., RF, SVM, ANN) were approximately higher than 91% for various land cover classifications which is comparable with present research. The results showed that RF had the best precision level of classification when compared with SVM, CT, and ANN models [73,61,62]. Therefore, this article only used the RF classification method, and we do not have a focus on evaluation of the performance of sequential classification method. The classification accuracy satisfies the standard measures proposed by Fielding and Bell [74]. In Yu et al.[75] research, images from Landsat 7 ETM+ and Landsat 8OLI were selected and they also used RF model which has been implemented by software named eCognition Developer 9.0. The overall accuracy was 86.7% which is lower than the accuracy level of the present study (93.75%). The reason may be due to the number of decision trees. This research originally set 100 decision trees while the accuracy is approximately equal to 85%, when we increased the number of decision trees to 400, the accuracy level rose to about 93%. The use of remotely sensed dataset depends upon the user's need, requirement, and type of assessment of the landscape. While other factors such as regional coverage (either large or small MODIS, MISR), spatial and spectral (AVIRIS, ASTER, AVHRR), high spatial-spectral resolution (AISA—airborne

hyperspectral images), temporal coverage (LANDSAT TM, MSS, ETM_p) and Synthetic Aperture Radar (SAR) data (to counter cloud effects) play an important role in choosing the particular data for a specific type of study. In this article, we selected Landsat images due to the fact that Landsat has a long orbit time and is convenient to collect images of long time series with cost-free, making it suitable for analysis over a large time span, and the resolution is 30m which is high enough for LULC classification. This issue was proved by Rodriguez-Galiano and Chica-Rivas [61].

4.3.2. Government policies

LULC change can be considerably influenced by government planning and industrial development policies. The 1.4-billion-person population of China faces significant food security and environmental challenges. The government has to encourage economic growth, enhance quality of life, and protect the environment. During periods of rapid economic expansion, housing, transportation, and industry will require more land. Large tracts of farmland and undeveloped land have been occupied, while the amount of land devoted to construction has risen sharply (Figure 4). During the period between 1992 and 2005, the rate of development in Jinan was relatively slow, resulting in a significant disparity between the municipal districts and other cities. Thus, the size of the impervious surface grew swiftly in the municipal districts (Figure 3 and Table 5) while it grew slowly in the remaining regions. The construction of Harmonious Jinan (COHJ) was established in 2005. This city was included in both the "Eleventh Five-Year" plan and the national development strategy. The COHJ became a master plan for development and boosting the economy. Since 2015, Jinan has identified "building four centers" as the core strategic goal of Jinan's construction and development, clearly proposing to make Jinan an important regional scientific and technological innovation center in the country. In addition, the "Three Year Plan" clearly proposed to accelerate the interconnection of transportation facilities, strengthen regional ties and cooperation, and jointly build the "The Belt and Road" land; These policies promote industrial cooperation among cities along the Yellow River and jointly build demonstration belts for industrial cooperation which will result in rapid development for the industrial and construction industries.

The traditional planning concept for Jinan's "central urban area" has been replaced with "main city." The eastern urban area, western urban area, and old urban area are named Dongcheng, Xicheng, and Zhongcheng, respectively. As a consequence, regional development primarily occurred in centralized areas, leading to the expansion of developed land in the connecting zones. These changes illustrate the significant impact of policies on regional land use and land cover modifications. The expansion of developed land has resulted in a significant loss of bare land, which is now the largest of the four types of land resources.

China has implemented several initiatives to preserve agricultural land to ensure food security. The most well-known program is the "Basic Farmland Protection System," which ensures China has at least 1.2 million km² of essential farmland available for agriculture and the nation's total food self-sufficiency. The alternative strategy, known as the "Balance of Arable Land" policy, requires that any conversion of arable land must be offset by the acquisition of land elsewhere. These land policies have postponed the loss of arable land. In the current study, we found that between 1992 and 2022, a sizeable percentage of impervious surface was converted into farmland (Tables 5 and 6). This finding is in line with other researchers' findings and may be explained by the terrain. Because Jinan is a plain region, it is more practical to convert developed land to farmland. This was significantly dissimilar from other areas, such as Nairobi, Kenya, and the Bale Mountains, Ethiopia, where farmland was primarily created by clearing existing vegetation [71]. Unused land should be carefully utilized considering it is a vital resource for the land reserve [72]. In urban growth, it's crucial to regulate the construction of new structures on farmed and unused land. Both the quantity and the quality of farmland should not be impacted, and the balance of farmed land must be properly managed.

In terms of sustainable LULC management, Jinan will assume a greater number of economic development responsibilities, thereby introducing new challenges. This study indicates that the main obstacles affecting the sustainable utilization of land resources in Jinan are the rapid increase in

impermeable water surface and the reduction of woodland (Figure 4). Moreover, the economy (urban population and GDP) and climate change were the primary drivers of LULC change (Tables 7 and 8). Therefore, departments tasked with the sustainable management of Jinan should prioritize the reasonable utilization of various types of impervious surface. Some new construction projects should first utilize existing impervious surface, strictly control new land, fully utilize unused land, and minimize the occupation of arable land. On the other hand, departments ought to regulate urban population growth and guarantee an appropriate range of GDP increase to enhance the use efficiency of impervious surface and the level of sustainable LULC. The policies of the government have a significant impact on regional LULC. The implementation of sustainable LULC policies by land management departments in Jinan will promote the effective utilization and long-term growth of regional land as well as enhance the level of regional land management.

Table 8. Linear relationships between land change and PCA for various types.

Impervious surface	Water	Farmland	Woodland	Bare land
$Y=3206.72+541.040$ $*F1$	$Y=95.99-$ $9.16*F1+0.9*F2$	$Y=2482.23-$ $198.40*F1+41.52$ $7*F1$	$Y=3438.612-$ $2.99*F1+50.61*F$ 2	$Y=979.17-$ $452.60*F1-$ $57.26*F2$
$R^2=0.748, P<0.05$	$R^2=0.013, P>0.05$	$R^2=0.046, P>0.05$	$R^2=0.577, P<0.05$	$R^2=0.660, P<0.05$

Future studies could use the data on LULC quantity and spatial distribution as the foundation for assessing Jinan's LULC sustainability. To evaluate the spatial variation in sustainable LULC in Jinan, the level of sustainable LULC will be determined. This will allow departments of land management to continue to develop their regional sustainable LULC policies.

5. Discussion

This study employed a model-based approach, along with Geographic Information System (GIS) and Remote Sensing (RS) tools, to quantitatively analyze the spatial-temporal changes in land-use and land-cover (LULC) distribution characteristics in Jinan. The study also investigated the variations in these characteristics and explored the factors driving these changes. Woodland is the most prevalent LULC type, followed by agricultural land and impervious surface. In 1992, these three LULC types comprised approximately 80.7% of Jinan's LULC area; by 2022, their proportion had risen to 99.9%. The extent of water had little impact on LULC modification. In 2022, impervious surface surpasses agricultural land as the most prevalent LULC. The area of bare land will decline from 18.9% in 1992 to 0.9% in 2022 at a rate of 60km²/year, while the area of impervious surface will increase from 23% in 1992 to 47% in 2022 at a rate of 81.5km²/year.

From the spatial characteristics of LULC change, farmland is primarily located in the northern part of Jinan City, including Shanghe, Jiyang, and Zhangqiu. From 1992 to 2022, the impervious surface in the northern part changed from scattered points around the cultivated land to a central part; The bar soil in the north has been converted into farmland and impervious surface; In addition, between 2002 and 2006, Woodland, located in the north, mainly transformed into arable land. The impervious surface in Jinan City, after 30 years of development, has expanded from the initial scattered impervious surface with only one center (1992) to the surrounding areas. In 2022, the scale of the impervious surface is twice the original area. The bare land and some woodland in Laiwu, located in the southeastern part of Jinan City, have been transformed into impervious surface. The distribution characteristics of these types of LULC in Jinan City in 2022 are as follows: Woodland is mainly distributed in the south, cultivated land is mainly distributed in the north, water has not changed significantly, and it is mainly the Yellow River that runs from east to west; The impervious surface area accounts for almost half of the total area, mainly located in the central and southeast directions.

From 1992 to 1998, according to the quantitative characteristics of LULC transfer, the type of cultivated land transfer was bare land, which was predominantly converted into impervious surface

and farmland. 44.8% of the transferred area was converted to impervious surface, accounting for 315.14 km²; 291.33 km² of the converted area into farmland accounts for 41.4% of the transferred area. During the three time periods of 1998, 2002, 2006, 2011, 2011, and 2017, the largest change in land conversion among various types in the region was in woodland, mainly converted into impervious surface. In addition, from 2002 to 2006, the impervious surface experienced the fastest growth, at approximately 506.45 km², and during these four years, the absolute value of the transfer area was higher, indicating more frequent transfers between these land types. For bare land, except for an increase from 1998 to 2002, it indicates that its transfer in was greater than that out, which may be related to relevant policies or climate change in that year. The area of bare land decreased in other research periods, it is mainly converted into impervious surface, with a small portion being used for agricultural and green land.

The normalized regression coefficients in the PCA test and regression are dimensionless units that can be applied to assess the extent of impact for all independent variables. The driving force analysis of LULC change reveals that the driving forces of impervious surface, woodland, bare land, agricultural land, and water body change were significantly different. In general, population, GDP, and climate change can be regarded as the main factors that have influenced LULC change. During the recent year, population and GDP have a positive correlation with impervious surface which means with the population increase and GDP growth, the government would like to develop more impervious surface (departments, houses, industries, facilities, etc.) to maintain economic development and meet population growth.

Government policies also impact LULC change. The formulation of the department has an immediate effect on regional LULC changes, such as the Construction of Harmonious Jinan (COHJ). The industry structure and regional development strategies influence LULC modification indirectly. In 2005, Jinan, for example, was included in The "Eleventh Five-Year Plan" which was established as a national development plan, subsequently accelerating the rate of changes in LULC within neighbouring regions. The transformation of LULC patterns necessitates a substantial investment of labour, resources, manpower, and capital; therefore, the government should be more comprehensive as well as wise in formulating land policies.

6. Conclusion

The availability of information regarding spatiotemporal land-use variation and city development status is crucial for effective land-use projection and decision-making. However, in many urban districts, like Jinan City, such data is often limited. In this study, LULC maps were derived from multi-temporal Landsat images, and spatial analysis techniques and statistical analysis were employed to analyze the spatial-temporal patterns of land-use variation and driving forces in Jinan City from 1992 to 2022.

The study findings revealed diverse trends in the changes of land-use and land-cover (LULC) types, with significant transitions observed from bare land and woodland to other types, particularly an increase in impervious surfaces over the course of 30 years. From the present research, the impervious surface of Jinan City expanded impervious surface is more than twice as large as before. The expansion rates were high and expanded from only concentrated on two districts to being significantly displayed in each district. Farmland and woodland were located in the northern and southern parts respectively and farmland experienced fluctuation while still staying stable in 2022 compared with 1992. The factors affecting the LULC change in Jinan were also discussed. They comprise the (GDP and population) climate, and the economy accounts for the main influencing factor for LULC changes.

The economy (GDP and population) and climate change are the primary drivers of the increase in developed land. The government should consider the carrying capacity of land when developing the economy to avoid overexploitation. Population agglomeration is substantially affected by LULC patterns. When developing LULC policies, the Department of Land Management ought to take into account rationally planning land resources to avoid excessive population concentration. When departments develop land development tactics, it is critical for them to concentrate on areas

experiencing rapid LULC change. To ensure adequate reserve land, the department of land management should, if necessary, limit the rate of LULC transfer in an area of volatile LULC change. In response to national low-carbon policies and to reduce harmful gas emissions, attention should also be paid to the climate-influencing factors of urban areas. Further studies on these issues are required. For example, issues such as the urban heat island effect, carbon emissions from impermeable surfaces, and the coupling relationship between urban land change and urban development can provide a basis and reference for sustainable urban development from a more comprehensive perspective. Researchers and stakeholders can refer to or base their further analyses on this information, which may require information about Land Use and Land Cover (LULC) support. They can also adjust certain parameters of Random Forests to potentially improve classification accuracy. Additionally, they can apply PCA tests to other areas in combination with other regression methods.

Author Contributions: Lingye Tan: Conceptualization, Methodology, Software, visualization and Writing-Original draft. Ziyang Zhang: Resources, Data curation, and Supervision. Robert L.K. Tiong and Mohammad Najafzadeh: Writing- Reviewing and Editing. All authors will be informed about each step of manuscript processing including submission, revision, revision reminder, etc. via emails from our system or assigned Assistant Editor.

Conflicts of Interest: The authors declare no conflicts of interest regarding the publication of this paper.

References

1. Lawler, J.J.; Lewis, D.J.; Nelson, E.; Plantinga, A.J.; Polasky, S.; Withey, J.C.; Helmers, D.P.; Martinuzzi, S.; Pennington, D.; Radeloff, V.C. Projected land-use change impacts on ecosystem services in the United States. *Proceedings of the National Academy of Sciences* **2014**, *111*, 7492-7497.
2. Wulder, M.A.; White, J.C.; Goward, S.N.; Masek, J.G.; Irons, J.R.; Herold, M.; Cohen, W.B.; Loveland, T.R.; Woodcock, C.E. Landsat continuity: Issues and opportunities for land cover monitoring. *Remote Sensing of Environment* **2008**, *112*, 955-969.
3. Mooney, H.A.; Duraipappah, A.; Larigauderie, A. Evolution of natural and social science interactions in global change research programs. *Proceedings of the National Academy of Sciences* **2013**, *110*, 3665-3672.
4. Zhu, Z.; Woodcock, C.E. Continuous change detection and classification of land cover using all available Landsat data. *Remote sensing of Environment* **2014**, *144*, 152-171.
5. Deng, L.; Liu, G.b.; Shangguan, Z.p. Land-use conversion and changing soil carbon stocks in China's 'Grain-for-Green' Program: a synthesis. *Global Change Biology* **2014**, *20*, 3544-3556.
6. Debnath, J.; Sahariah, D.; Lahon, D.; Nath, N.; Chand, K.; Meraj, G.; Farooq, M.; Kumar, P.; Kanga, S.; Singh, S.K. Geospatial modeling to assess the past and future land use-land cover changes in the Brahmaputra Valley, NE India, for sustainable land resource management. *Environmental Science and Pollution Research* **2022**, 1-24.
7. Jin, X.; Jiang, P.; Ma, D.; Li, M. Land system evolution of Qinghai-Tibetan Plateau under various development strategies. *Applied Geography* **2019**, *104*, 1-9.
8. Gaur, S.; Singh, R. A comprehensive review on land use/land cover (LULC) change modeling for urban development: current status and future prospects. *Sustainability* **2023**, *15*, 903.
9. Wear, D.N.; Bolstad, P. Land-use changes in southern Appalachian landscapes: spatial analysis and forecast evaluation. *Ecosystems* **1998**, *1*, 575-594.
10. Yu, X.; Yang, G. The advances and problems of land use and land cover change research in China. *Progress in Geography* **2002**, *21*, 51-57.
11. Hietel, E.; Waldhardt, R.; Otte, A. Analysing land-cover changes in relation to environmental variables in Hesse, Germany. *Landscape ecology* **2004**, *19*, 473-489.

12. Zhu, L.; Song, R.; Sun, S.; Li, Y.; Hu, K. Land use/land cover change and its impact on ecosystem carbon storage in coastal areas of China from 1980 to 2050. *Ecological Indicators* **2022**, *142*, 109178.
13. Wang, Z.-J.; Liu, S.-J.; Li, J.-H.; Pan, C.; Wu, J.-L.; Ran, J.; Su, Y. Remarkable improvement of ecosystem service values promoted by land use/land cover changes on the Yungui Plateau of China during 2001–2020. *Ecological Indicators* **2022**, *142*, 109303.
14. Zhang, D.; Wang, X.; Qu, L.; Li, S.; Lin, Y.; Yao, R.; Zhou, X.; Li, J. Land use/cover predictions incorporating ecological security for the Yangtze River Delta region, China. *Ecological Indicators* **2020**, *119*, 106841.
15. Yin, J.; Yin, Z.; Zhong, H.; Xu, S.; Hu, X.; Wang, J.; Wu, J. Monitoring urban expansion and land use/land cover changes of Shanghai metropolitan area during the transitional economy (1979–2009) in China. *Environmental monitoring and assessment* **2011**, *177*, 609–621.
16. Ding, H.; Shi, W. Land-use/land-cover change and its influence on surface temperature: a case study in Beijing City. *International Journal of Remote Sensing* **2013**, *34*, 5503–5517.
17. Wu, Y.; Li, S.; Yu, S. Monitoring urban expansion and its effects on land use and land cover changes in Guangzhou city, China. *Environmental monitoring and assessment* **2016**, *188*, 1–15.
18. Sanderson, E.W.; Jaiteh, M.; Levy, M.A.; Redford, K.H.; Wannebo, A.V.; Woolmer, G. The human footprint and the last of the wild: the human footprint is a global map of human influence on the land surface, which suggests that human beings are stewards of nature, whether we like it or not. *BioScience* **2002**, *52*, 891–904.
19. Hersperger, A.M.; Bürgi, M. Going beyond landscape change description: Quantifying the importance of driving forces of landscape change in a Central Europe case study. *Land Use Policy* **2009**, *26*, 640–648.
20. Arifasihati, Y. Analysis of land use and cover changes in Ciliwung and Cisadane Watershed in three decades. *Procedia Environmental Sciences* **2016**, *33*, 465–469.
21. Tavares, A.O.; Monteiro, M.; Barros, J.L.; Santos, P.P. Long-term land-use changes in small/medium-sized cities. Enhancing the general trends and local characteristics. *European Planning Studies* **2019**, *27*, 1432–1459.
22. Nagy, R.C.; Lockaby, B.G. Urbanization in the Southeastern United States: Socioeconomic forces and ecological responses along an urban-rural gradient. *Urban Ecosystems* **2011**, *14*, 71–86.
23. Tiitu, M. Expansion of the built-up areas in Finnish city regions—The approach of travel-related urban zones. *Applied Geography* **2018**, *101*, 1–13.
24. De la Luz Hernández-Flores, M.; Otaño-Sánchez, E.M.; Galeana-Pizana, M.; Roldán-Cruz, E.I.; Razo-Zárate, R.; González-Ramírez, C.A.; Galindo-Castillo, E.; Gordillo-Martínez, A.J. Urban driving forces and megacity expansion threats. Study case in the Mexico City periphery. *Habitat International* **2017**, *64*, 109–122.
25. Xu, Y.; McNamara, P.; Wu, Y.; Dong, Y. An econometric analysis of changes in arable land utilization using multinomial logit model in Pinggu district, Beijing, China. *Journal of environmental management* **2013**, *128*, 324–334.
26. Islam, M.D.; Islam, K.S.; Ahasan, R.; Mia, M.R.; Haque, M.E. A data-driven machine learning-based approach for urban land cover change modeling: A case of Khulna City Corporation area. *Remote Sensing Applications: Society and Environment* **2021**, *24*, 100634.
27. Essien, E.; Cyrus, S. Detection of urban development in Uyo (Nigeria) using remote sensing. *Land* **2019**, *8*, 102.
28. Turner, R.K.; Adger, W.N.; Doktor, N. *Key issues in the economics of sea level rise*; Centre for Social and Economic Research on the Global Environment: 1993.
29. Stephen, D.; David, J.; Anand, P. Conflicting interests in the use of Kerala's penaeid shrimp resources: A case in question. *Journal of the Marine Biological Association of India* **1993**, *35*, 29–38.

30. Briassoulis, H.; van der Straaten, J. Tourism and the environment: An overview. *Tourism and the environment: Regional, economic, cultural and policy issues* **2000**, 1-19.
31. Xie, Y.; Mei, Y.; Guangjin, T.; Xuerong, X. Socio-economic driving forces of arable land conversion: A case study of Wuxian City, China. *Global Environmental Change* **2005**, *15*, 238-252.
32. Lu, D.; Li, G.; Moran, E.; Dutra, L.; Batistella, M. A comparison of multisensor integration methods for land cover classification in the Brazilian Amazon. *GIScience & Remote Sensing* **2011**, *48*, 345-370.
33. Shao, Y.; Lunetta, R.S. Comparison of support vector machine, neural network, and CART algorithms for the land-cover classification using limited training data points. *ISPRS Journal of Photogrammetry and Remote Sensing* **2012**, *70*, 78-87.
34. Thanh Noi, P.; Kappas, M. Comparison of random forest, k-nearest neighbor, and support vector machine classifiers for land cover classification using Sentinel-2 imagery. *Sensors* **2017**, *18*, 18.
35. Toure, S.I.; Stow, D.A.; Shih, H.-c.; Weeks, J.; Lopez-Carr, D. Land cover and land use change analysis using multi-spatial resolution data and object-based image analysis. *Remote Sensing of Environment* **2018**, *210*, 259-268.
36. Wu, Q.; Li, H.-q.; Wang, R.-s.; Paulussen, J.; He, Y.; Wang, M.; Wang, B.-h.; Wang, Z. Monitoring and predicting land use change in Beijing using remote sensing and GIS. *Landscape and urban planning* **2006**, *78*, 322-333.
37. Rawat, J.; Kumar, M. Monitoring land use/cover change using remote sensing and GIS techniques: A case study of Hawalbagh block, district Almora, Uttarakhand, India. *The Egyptian Journal of Remote Sensing and Space Science* **2015**, *18*, 77-84.
38. Tadese, M.; Kumar, L.; Koech, R.; Kogo, B.K. Mapping of land-use/land-cover changes and its dynamics in Awash River Basin using remote sensing and GIS. *Remote Sensing Applications: Society and Environment* **2020**, *19*, 100352.
39. Sánchez-Cuervo, A.M.; Aide, T.M.; Clark, M.L.; Etter, A. Land cover change in Colombia: surprising forest recovery trends between 2001 and 2010. **2012**.
40. Schoeman, F.; Newby, T.; Thompson, M.; Van den Berg, E.C. South African national land-cover change map. *South African Journal of Geomatics* **2013**, *2*, 94-105.
41. Jiyuan, L.; Mingliang, L.; Xiangzheng, D.; Dafang, Z.; Zengxiang, Z.; Di, L. The land use and land cover change database and its relative studies in China. *Journal of Geographical Sciences* **2002**, *12*, 275-282.
42. Li, J.; Wang, Z.; Lai, C.; Wu, X.; Zeng, Z.; Chen, X.; Lian, Y. Response of net primary production to land use and land cover change in mainland China since the late 1980s. *Science of the Total Environment* **2018**, *639*, 237-247.
43. Wen, C.; Dong, W.; Meng, Y.; Li, C.; Zhang, Q. Application of a loose coupling model for assessing the impact of land-cover changes on groundwater recharge in the Jinan spring area, China. *Environmental Earth Sciences* **2019**, *78*, 1-17.
44. Sun, L.; Wei, J.; Duan, D.; Guo, Y.; Yang, D.; Jia, C.; Mi, X. Impact of Land-Use and Land-Cover Change on urban air quality in representative cities of China. *Journal of Atmospheric and Solar-Terrestrial Physics* **2016**, *142*, 43-54.
45. Feng, R.; Wang, K. Spatiotemporal effects of administrative division adjustment on urban expansion in China. *Land Use Policy* **2021**, *101*, 105143.
46. Kontgis, C.; Schneider, A.; Fox, J.; Saksena, S.; Spencer, J.H.; Castrence, M. Monitoring peri-urbanization in the greater Ho Chi Minh City metropolitan area. *Applied Geography* **2014**, *53*, 377-388.

47. Nassar, A.K.; Blackburn, G.A.; Whyatt, J.D. Developing the desert: The pace and process of urban growth in Dubai. *Computers, Environment and Urban Systems* **2014**, *45*, 50-62.
48. Dai, E.; Wu, Z.; Du, X. A gradient analysis on urban sprawl and urban landscape pattern between 1985 and 2000 in the Pearl River Delta, China. *Frontiers of Earth Science* **2018**, *12*, 791-807.
49. Feng, R.; Wang, K. The direct and lag effects of administrative division adjustment on urban expansion patterns in Chinese mega-urban agglomerations. *Land Use Policy* **2022**, *112*, 105805.
50. Whiteside, H. Privatizing Canadian government land and real estate: Railroads, reconciliation, and rip-offs. *Land Use Policy* **2020**, *99*, 104821.
51. Zhang, S.; De Roo, G.; Van Dijk, T. Urban land changes as the interaction between self-organization and institutions. *Planning Practice and Research* **2015**, *30*, 160-178.
52. Adam, A.G. Thinking outside the box and introducing land readjustment against the conventional urban land acquisition and delivery method in Ethiopia. *Land use policy* **2019**, *81*, 624-631.
53. Dewan, A.M.; Yamaguchi, Y. Using remote sensing and GIS to detect and monitor land use and land cover change in Dhaka Metropolitan of Bangladesh during 1960–2005. *Environmental monitoring and assessment* **2009**, *150*, 237-249.
54. Tendaupenyu, P.; Magadza, C.H.D.; Murwira, A. Changes in landuse/landcover patterns and human population growth in the Lake Chivero catchment, Zimbabwe. *Geocarto International* **2017**, *32*, 797-811.
55. Pourazar, H.; Samadzadegan, F.; Dadrass Javan, F. Aerial multispectral imagery for plant disease detection: Radiometric calibration necessity assessment. *European Journal of Remote Sensing* **2019**, *52*, 17-31.
56. Chen, J.; He, C.; Yue, C. Atmospheric correction of an Advance Land Imager (ALI) image based on the FLAASH module. *Journal of Zhejiang A&F University* **2011**, *28*, 590-596.
57. Li, X.; Chen, W.; Cheng, X.; Wang, L. A comparison of machine learning algorithms for mapping of complex surface-mined and agricultural landscapes using ZiYuan-3 stereo satellite imagery. *Remote sensing* **2016**, *8*, 514.
58. Millard, K.; Richardson, M. On the importance of training data sample selection in random forest image classification: A case study in peatland ecosystem mapping. *Remote sensing* **2015**, *7*, 8489-8515.
59. Maxwell, A.E.; Strager, M.P.; Warner, T.A.; Ramezan, C.A.; Morgan, A.N.; Pauley, C.E. Large-area, high spatial resolution land cover mapping using random forests, GEOBIA, and NAIP orthophotography: Findings and recommendations. *Remote Sensing* **2019**, *11*, 1409.
60. Teluguntla, P.; Thenkabail, P.S.; Oliphant, A.; Xiong, J.; Gumma, M.K.; Congalton, R.G.; Yadav, K.; Huete, A. A 30-m landsat-derived cropland extent product of Australia and China using random forest machine learning algorithm on Google Earth Engine cloud computing platform. *ISPRS journal of photogrammetry and remote sensing* **2018**, *144*, 325-340.
61. Rodriguez-Galiano, V.F.; Chica-Rivas, M. Evaluation of different machine learning methods for land cover mapping of a Mediterranean area using multi-seasonal Landsat images and Digital Terrain Models. *International Journal of Digital Earth* **2014**, *7*, 492-509.
62. Abdel-Rahman, E.M.; Mutanga, O.; Adam, E.; Ismail, R. Detecting Sirex noctilio grey-attacked and lightning-struck pine trees using airborne hyperspectral data, random forest and support vector machines classifiers. *ISPRS Journal of Photogrammetry and Remote Sensing* **2014**, *88*, 48-59.
63. Van Beijma, S.; Comber, A.; Lamb, A. Random forest classification of salt marsh vegetation habitats using quad-polarimetric airborne SAR, elevation and optical RS data. *Remote Sensing of Environment* **2014**, *149*, 118-129.
64. Breiman, L. Random forests. *Machine learning* **2001**, *45*, 5-32.

65. Hastie, T.; Tibshirani, R.; Friedman, J.H.; Friedman, J.H. *The elements of statistical learning: data mining, inference, and prediction*; Springer: 2009; Volume 2.
66. Congalton, R.G. A review of assessing the accuracy of classifications of remotely sensed data. *Remote sensing of environment* **1991**, *37*, 35-46.
67. Voss, M.; Sugumaran, R. Seasonal effect on tree species classification in an urban environment using hyperspectral data, LiDAR, and an object-oriented approach. *Sensors* **2008**, *8*, 3020-3036.
68. Ge, Y.; Zhang, K.; Yang, X. A 110-year pollen record of land use and land cover changes in an anthropogenic watershed landscape, eastern China: Understanding past human-environment interactions. *Science of the Total Environment* **2019**, *650*, 2906-2918.
69. Van Asselen, S.; Verburg, P.H. Land cover change or land-use intensification: simulating land system change with a global-scale land change model. *Global change biology* **2013**, *19*, 3648-3667.
70. Zhou, Y.; Li, Y.; Xu, C. Land consolidation and rural revitalization in China: Mechanisms and paths. *Land Use Policy* **2020**, *91*, 104379.
71. Du, X.; Jin, X.; Yang, X.; Yang, X.; Zhou, Y. Spatial pattern of land use change and its driving force in Jiangsu Province. *International journal of environmental research and public health* **2014**, *11*, 3215-3232.
72. Li, M.; Zhou, Y.; Xiao, P.; Tian, Y.; Huang, H.; Xiao, L. Evolution of Habitat Quality and Its Topographic Gradient Effect in Northwest Hubei Province from 2000 to 2020 Based on the InVEST Model. *Land* **2021**, *10*, 857.
73. Talukdar, S.; Singha, P.; Mahato, S.; Pal, S.; Liou, Y.-A.; Rahman, A. Land-use land-cover classification by machine learning classifiers for satellite observations—A review. *Remote Sensing* **2020**, *12*, 1135.
74. Fielding, A.H.; Bell, J.F. A review of methods for the assessment of prediction errors in conservation presence/absence models. *Environmental Conservation* **1997**, *24*, 38-49.
75. Yu, G.; Liu, T.; Wang, Q.; Li, T.; Li, X.; Song, G.; Feng, Y. Impact of Land Use/Land Cover Change on Ecological Quality during Urbanization in the Lower Yellow River Basin: A Case Study of Jinan City. *Remote Sensing* **2022**, *14*, 6273.

Disclaimer/Publisher's Note: The statements, opinions and data contained in all publications are solely those of the individual author(s) and contributor(s) and not of MDPI and/or the editor(s). MDPI and/or the editor(s) disclaim responsibility for any injury to people or property resulting from any ideas, methods, instructions or products referred to in the content.